18th Australasian Fluid Mechanics Conference
Launceston, Australia
3-7 December 2012

Computing optimal flow disturbances

H. M. Blackburn[1], **X. Mao**[1,2] **and S. J. Sherwin**[3]

[1]Department of Mechanical and Aerospace Engineering
Monash University, Victoria 3800, Australia

[2]School of Engineering and Computer Science
Durham University, Durham DH1 3LE, UK

[3]Department of Aeronautics
Imperial College London, South Kensington SW7 2BY, UK

Abstract

We outline methodologies for computation of the spatial distributions of energy-optimal linear initial and boundary disturbances to incompressible flows. The theory presented here is based in techniques developed for constrained optimisation, but we show that there are equivalent eigenvalue interpretations. As a result the computations may be carried out either by optimisation or eigensystem methods, leading to the same outcomes though typically the eigensystem approaches converge more rapidly for optimal initial condition calculations. We show how the methods have been applied to example open flows.

Introduction

Methods for computing linear large-time stability and optimal initial condition disturbances for transient growth in general incompressible flows are now well established (see e.g. [1, 15]). For open flows (ones with an inflow and an outflow) one may well be more interested in finding an inflow disturbance which can lead to energetic disturbances further downstream than in optimal initial disturbances: it is rather difficult to conceive how an initial disturbance could actually be created within an open flow.

We here discuss how to compute optimal inflow boundary condition perturbations, those that produce an optimal gain, i.e. kinetic energy in the domain at a given time horizon normalised by a measure of time-integrated energy on the inflow boundary segment. The conceptual setting for these discussions lies in the arena of optimal flow control, as described e.g. in [8, 13]. From consideration of suitable constrained optimisation problems, we show that one can compute either optimal initial or boundary condition perturbations to prescribed base flows $(\boldsymbol{U},P)$ using iterative gradient-based methods. However, further consideration also shows that in each case there is an equivalent eigenvalue problem which delivers the same perturbation. We examine the relative computational efficiencies of these two alternative approaches.

We demonstrate that, similarly to the optimal initial condition problem, the gain can be interpreted as the leading singular value of the forward linearized operator that evolves the boundary conditions to the final state at a fixed time. In this investigation we restrict our attention to problems where the temporal profile of the perturbations examined is a product of a Gaussian bell and a sinusoid, whose frequency is selected to excite axial wavelengths similar to those of the optimal initial perturbations in the same geometry. Comparison of the final state induced by the optimal boundary perturbation with that induced by the optimal initial condition demonstrates a close agreement for the selected problem. Previous works dealing with optimal boundary perturbation, e.g. [7] considered a prescribed spatial structure and computed an optimal temporal variation of a wall-normal velocity component, whereas here we consider perturbations with a prescribed temporal structure and compute the optimal spatial variation of velocity boundary conditions over a one-dimensional inflow boundary segment. The methodology is capable of finding optimal boundary condition perturbations in general non-parallel two- and three-dimensional flows. The gradient-based optimisation approach to these problems has been described in an earlier paper [11], but here more consideration is given to comparing optimisation and eigensystem methodologies.

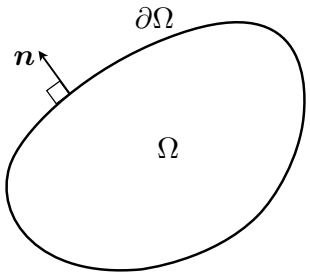

Figure 1: Schematic representation of a spatial flow domain Ω, boundary $\partial\Omega$ and unit outward normal vector $\boldsymbol{n}$.

The optimal boundary perturbation problem is, in the flows examined to date at least, closely linked to the optimal initial condition problem in that ultimately the same physics are excited and the wave-packet nature of the optimal inflow perturbation is closely linked to that for the optimal initial disturbance and outcome.

Problem definition

Working from the incompressible Navier–Stokes equations

$$\partial_t \boldsymbol{u} = -\boldsymbol{u}\cdot\boldsymbol{\nabla}\boldsymbol{u} - \boldsymbol{\nabla}p + Re^{-1}\nabla^2\boldsymbol{u}, \quad \text{with} \quad \boldsymbol{\nabla}\cdot\boldsymbol{u} = 0,$$

where p is the modified or kinematic pressure, $\boldsymbol{u}$ is the velocity vector, while the Reynolds number $Re = UD/\nu$ where U and D are convenient velocity and length scales and ν is kinematic viscosity. Decomposing the flow field as the sum of a base flow and a perturbation i.e. $(\boldsymbol{u},p) = (\boldsymbol{U},P) + (\boldsymbol{u}',p')$ and omitting the interaction of perturbations, we obtain the linearized Navier–Stokes (LNS) equations, which govern the evolution of infinitesimal perturbations, as

$$\partial_t \boldsymbol{u}' = -\boldsymbol{U}\cdot\boldsymbol{\nabla}\boldsymbol{u}' - (\boldsymbol{\nabla}\boldsymbol{U})^T\cdot\boldsymbol{u}' - \boldsymbol{\nabla}p' + Re^{-1}\nabla^2\boldsymbol{u}', \text{ with } \boldsymbol{\nabla}\cdot\boldsymbol{u}' = 0,$$

or more compactly, considering that pressure is a dependent variable in an incompressible flow,

$$\partial_t \boldsymbol{u}' - L(\boldsymbol{u}') = 0. \tag{1}$$

Flow is considered within a spatial domain Ω which has a boundary surface $\partial\Omega$ and unit outward normal $\boldsymbol{n}$, as indicated in figure 1. Flow is taken to evolve over the time interval $[0,\tau]$, so the space-time domain considered is $\Omega\times[0,\tau]$.

We introduce scalar products defined on spatial domain Ω and its boundary $\partial\Omega$

$$(\boldsymbol{a},\boldsymbol{b})=\int_\Omega \boldsymbol{a}\cdot\boldsymbol{b}\,\mathrm{d}V, \qquad \langle\boldsymbol{a},\boldsymbol{b}\rangle=\int_0^\tau\int_\Omega \boldsymbol{a}\cdot\boldsymbol{b}\,\mathrm{d}V\mathrm{d}t,$$
$$[\boldsymbol{c},\boldsymbol{d}]=D\int_{\partial\Omega} \boldsymbol{c}\cdot\boldsymbol{d}\,\mathrm{d}S, \qquad \{\boldsymbol{c},\boldsymbol{d}\}=D\int_0^\tau\int_{\partial\Omega} \boldsymbol{c}\cdot\boldsymbol{d}\,\mathrm{d}S\mathrm{d}t,$$

where $\boldsymbol{a},\boldsymbol{b}\in\Omega\times[0,\tau]$ and $\boldsymbol{c},\boldsymbol{d}\in\partial\Omega\times[0,\tau]$. Ω is the spatial domain and $\partial\Omega$ is the spatial boundary. Length scale D is introduced into these definitions in order to maintain dimensional homogeneity.

By considering the space-time inner product of the linearized Navier–Stokes equations with adjoint velocity and pressure fields $(\boldsymbol{u}^*,p^*)$ and using integration by parts (but in conditions where the perturbation and adjoint variables have compact support in both space and time, see [1]) we obtain the adjoint Navier–Stokes equations (ANS) as

$$-\partial_t\boldsymbol{u}^*=-\boldsymbol{U}\cdot\boldsymbol{\nabla}\boldsymbol{u}^*+\boldsymbol{\nabla}\boldsymbol{U}\cdot\boldsymbol{u}^*-\boldsymbol{\nabla}p^*+Re^{-1}\nabla^2\boldsymbol{u}^*,\quad \boldsymbol{\nabla}\cdot\boldsymbol{u}^*=0,$$

which are required to be integrated backwards in time owing to the change in sign on the temporal derivative; a forwards integration would conversely imply negative diffusion. Again, for convenience, we introduce a compact form for these equations:

$$\partial_t\boldsymbol{u}^*+L^*(\boldsymbol{u}^*)=0. \tag{2}$$

The optimal initial condition problem can be expressed as seeking an initial perturbation to maximise the energy growth over time interval τ, defined as the ratio of final energy at time τ and the initial energy at time 0 and denoted as G; the optimal boundary condition problem can be expressed as seeking the boundary perturbations to maximise the gain, defined as the ratio of final energy at time τ and a measurement of the boundary perturbation, denoted as K. Hence

$$G=\max_{\boldsymbol{u}_0}\frac{(\boldsymbol{u}'_\tau,\boldsymbol{u}'_\tau)}{(\boldsymbol{u}'_0,\boldsymbol{u}'_0)} \qquad\text{and}\qquad K=\max_{\boldsymbol{u}_c}\frac{(\boldsymbol{u}'_\tau,\boldsymbol{u}'_\tau)}{\{\boldsymbol{u}'_c,\boldsymbol{u}'_c\}}, \tag{3}$$

where $\boldsymbol{u}'_0\in\Omega$ denotes the initial perturbation velocity vector, $\boldsymbol{u}'_c\in\partial\Omega$ represents the (controlled sector) boundary velocity vector and $\boldsymbol{u}'_\tau\in\Omega$ is the response velocity vector at time τ. In the initial value problem we set the boundary perturbation to zero, while in the boundary value problem we set the initial perturbation to zero in order to isolate the developments of initial and boundary perturbations and make the ratios G and K independent of the magnitude of initial or boundary perturbations.

To reduce the dimension of $\boldsymbol{u}'_c$, we separate the spatial and temporal dependencies and specify the temporal dependency explicitly, such that e.g.

$$\boldsymbol{u}'_c(\boldsymbol{x},t)=\hat{\boldsymbol{u}}_c(\boldsymbol{x})f(t,\omega). \tag{4}$$

The function $f(t,\omega)$ contains terms to eliminate temporal and spatial discontinuity when integrating the governing equations, as shown for example in figure 2. When the final time τ is large enough, this decomposition tends to the Fourier decomposition with ω acting as the frequency. Therefore in the optimal boundary problem, we only optimise the spatial dependency function $\hat{\boldsymbol{u}}_c(\boldsymbol{x})$. Correspondingly the object to maximise becomes

$$K=\max_{\hat{\boldsymbol{u}}_c}\frac{(\boldsymbol{u}'_\tau,\boldsymbol{u}'_\tau)}{[\hat{\boldsymbol{u}}_c,\hat{\boldsymbol{u}}_c]}$$

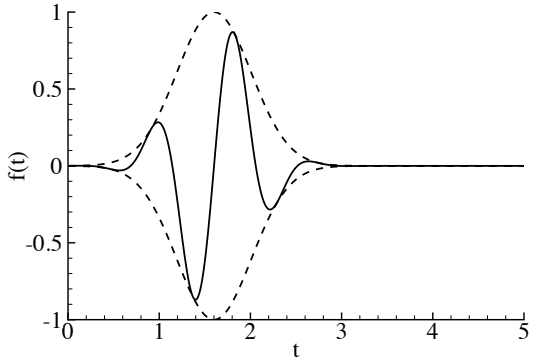

Figure 2: Example time-dependency of a controlled velocity boundary condition, see (4).

where we observe that $f(t,\omega)$ is spatially constant and has the effect of uniformly scaling $\boldsymbol{u}'_\tau$ and so is not included. Note that K is dimensionless regardless of the system of spatial measurement adopted, but is now particular to the choice of $f(t,\omega)$.

If the base flow is homogeneous in (say) the azimuthal direction θ for cylindrical coordinates (z,r,θ), we can further decompose the perturbation field into azimuthal Fourier modes, each of which will evolve independently under the assumption of linearity, such that:

$$(\boldsymbol{u}',p')=(u',v',w',p')=$$
$$[u'_m(r,z),v'_m(r,z),w'_m(r,z),p'_m(r,z)]\exp(\mathrm{i}m\theta),$$

where m denotes an integer azimuthal wavenumber. If the base flow is homogeneous in the spanwise direction in a Cartesian coordinate, a similar spanwise Fourier mode can be defined at a real spanwise wavenumber. We note that provided the Fourier mode index $m>0$, the controlled boundary has zero net mass flux at all times. To keep notation reasonably compact in what follows we implicitly adopt Fourier decomposition for the perturbation field, only introduce its azimuthal/spanwise Fourier mode index m when required, and suppress representation of θ-dependence.

Overview of optimisation methodology

The ratios G or K in (3) are, in the language of optimisation, cost or objective functionals which we can generalise as $\mathcal{J}(\boldsymbol{u}'_{\mathrm{opt}})$ where $\boldsymbol{u}'_{\mathrm{opt}}$ represents either an optimal initial or boundary velocity perturbation. We seek to maximize the ratios $\mathcal{J}(\boldsymbol{u}'_{\mathrm{opt}})$ through suitable choices of $\boldsymbol{u}'_{\mathrm{opt}}$. These functionals are to be optimised subject to the constraint that the perturbation velocity evolves in a way that satisfies its state equation, i.e. (1). The mechanism of Lagrange multipliers is invoked in order to convert the constrained optimisation problems into unconstrained optimisation problems [8, 13], in which the adjoint variables $(\boldsymbol{u}^*,p^*)$ take the roles of Lagrange multipliers with respect to the linearized Navier–Stokes equations:

$$\mathcal{L}=\mathcal{J}(\boldsymbol{u}'_{\mathrm{opt}})-\langle\boldsymbol{u}^*,\partial_t\boldsymbol{u}'-L(\boldsymbol{u}')\rangle. \tag{5}$$

The constrained optimisation task is then to seek stationary points of the Lagrangian functional $\mathcal{L}$ with respect to arbitrary variations in the control variable, $\delta\boldsymbol{u}'_{\mathrm{opt}}$, as well as of the state variable, $\delta\boldsymbol{u}'$, adjoint variable, $\delta\boldsymbol{u}^*$, and of the variable in the numerator of the objective functional, the terminal velocity field at time horizon τ, i.e. $\delta\boldsymbol{u}'_\tau$. The standard methodology here is to

employ the Gâteaux differential ([7, 8, 13])

$$\frac{\delta\mathcal{L}}{\delta\boldsymbol{q}} = \lim_{\varepsilon\to 0}\frac{\mathcal{L}(\boldsymbol{q}+\varepsilon\delta\boldsymbol{q})-\mathcal{L}(\boldsymbol{q})}{\varepsilon} \equiv \langle\nabla_{\boldsymbol{q}}\mathcal{L},\delta\boldsymbol{q}\rangle, \tag{6}$$

where $\boldsymbol{q}$ is any of the optimisation variables and δ represents an arbitrary variation. The final inner product is taken as appropriate to the variable whose variation is under consideration and is used as a definition in order to obtain a gradient of $\mathcal{L}$ with respect to the optimisation target variable (i.e. here either $\boldsymbol{u}'_0$ or $\hat{\boldsymbol{u}}_c$) for gradient-based optimisation.

In order to be able to take arbitrary variations with respect to the state variable $\boldsymbol{u}'$ we will need to remove spatio-temporal derivatives on that variable which are seen in (5). In this case we need to more fully consider the role of initial and boundary conditions. If we use integration by parts on the last term in (5) we obtain (see [1])

$$\begin{aligned}-\langle\boldsymbol{u}^*,\partial_t\boldsymbol{u}'-L(\boldsymbol{u}')\rangle &= \langle\boldsymbol{u}',\partial_t\boldsymbol{u}^*+L^*(\boldsymbol{u}^*)\rangle\\ &\quad+\int_0^\tau\int_\Omega -\partial_t(\boldsymbol{u}'\cdot\boldsymbol{u}^*)\,\mathrm{d}V\mathrm{d}t\\ &\quad+\int_0^\tau\int_\Omega \boldsymbol{\nabla}\cdot[-\boldsymbol{U}(\boldsymbol{u}'\cdot\boldsymbol{u}^*)+\boldsymbol{u}'p^*-\boldsymbol{u}^*p'\\ &\qquad+Re^{-1}(\boldsymbol{\nabla}\boldsymbol{u}'\cdot\boldsymbol{u}^*-\boldsymbol{\nabla}\boldsymbol{u}^*\cdot\boldsymbol{u}')]\,\mathrm{d}V\mathrm{d}t,\end{aligned} \tag{7}$$

which can be restated using only space-time boundary terms via an exchange of the order of integrations in one integral and the divergence theorem in another as

$$\begin{aligned}-\langle\boldsymbol{u}^*,\partial_t\boldsymbol{u}'-L(\boldsymbol{u}')\rangle &= \langle\boldsymbol{u}',\partial_t\boldsymbol{u}^*+L^*(\boldsymbol{u}^*)\rangle\\ &\quad-(\boldsymbol{u}^*_\tau,\boldsymbol{u}'_\tau)+(\boldsymbol{u}^*_0,\boldsymbol{u}'_0)\\ &\quad+\int_0^\tau\int_{\partial\Omega}\boldsymbol{n}\cdot[-\boldsymbol{U}(\boldsymbol{u}\cdot\boldsymbol{u}^*)+\boldsymbol{u}'p^*-\boldsymbol{u}^*p'\\ &\qquad+Re^{-1}(\boldsymbol{\nabla}\boldsymbol{u}^*\cdot\boldsymbol{u}'-\boldsymbol{\nabla}\boldsymbol{u}^*\cdot\boldsymbol{u}')]\,\mathrm{d}S\mathrm{d}t,\end{aligned} \tag{8}$$

where $\boldsymbol{n}$ is a unit outward normal vector on the boundary of the domain, $\partial\Omega$, see figure 1.

The particulars of the optimisation strategies to be pursued then depend on the terms retained in (8) according to whether we wish to compute optimal initial or boundary condition perturbations.

Optimal initial perturbations

When calculating optimal initial perturbations, the boundary velocity perturbations may set to zero, which is quite satisfactory if the flow domain is taken large enough that the direct and adjoint velocity perturbations are well contained within it for $t\in[0,\tau]$ and if any walls are zero-slip.

Optimisation approach

The optimisation approach to finding optimal initial perturbations was historically the first, as outlined e.g. in [15].

Adopting zero-Dirichlet boundary conditions for the velocity components for both LNS equations and the adjoint equations, the last integral in (8) becomes zero, and therefore

$$\mathcal{L}_0 = \frac{(\boldsymbol{u}'_\tau,\boldsymbol{u}'_\tau)}{(\boldsymbol{u}'_0,\boldsymbol{u}'_0)}+\langle\boldsymbol{u}^*,\partial_t\boldsymbol{u}'+L(\boldsymbol{u}')\rangle, \tag{9}$$

$$\begin{aligned}&\equiv\frac{(\boldsymbol{u}'_\tau,\boldsymbol{u}'_\tau)}{(\boldsymbol{u}'_0,\boldsymbol{u}'_0)}+\langle\boldsymbol{u}',\partial_t\boldsymbol{u}^*+L^*(\boldsymbol{u}^*)\rangle\\ &\qquad-(\boldsymbol{u}^*_\tau,\boldsymbol{u}'_\tau)+(\boldsymbol{u}^*_0,\boldsymbol{u}'_0).\end{aligned} \tag{10}$$

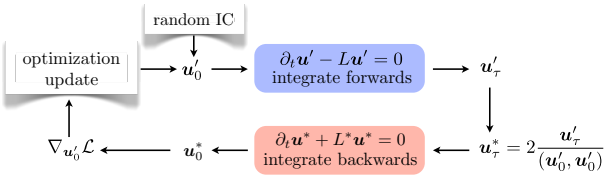

Figure 3: Optimisation-based strategy for finding optimal initial conditions. See also [15].

Setting to zero the first variations of $\mathcal{L}_0$ with respect to its independent variables $\boldsymbol{u}^*$, $\boldsymbol{u}'$ and $\boldsymbol{u}'_\tau$ yields the following set of equations:

$$\frac{\delta\mathcal{L}_0}{\delta\boldsymbol{u}^*}=0 \quad\Longrightarrow\quad \partial_t\boldsymbol{u}'-L(\boldsymbol{u}')=0, \tag{11}$$

$$\frac{\delta\mathcal{L}_0}{\delta\boldsymbol{u}'}=0 \quad\Longrightarrow\quad \partial_t\boldsymbol{u}^*+L^*(\boldsymbol{u}^*)=0, \tag{12}$$

$$\frac{\delta\mathcal{L}_0}{\delta\boldsymbol{u}'_\tau}=0 \quad\Longrightarrow\quad \boldsymbol{u}^*_\tau=\frac{2\boldsymbol{u}'_\tau}{(\boldsymbol{u}'_0,\boldsymbol{u}'_0)}. \tag{13}$$

The first two equations recover the LNS and ANS equations, while the third initialises the adjoint equations at $t=\tau$ with the scaled final condition of the LNS equations since the adjoint equations are integrated backwards. The LNS and ANS equations are integrated forwards and backwards respectively over time interval τ in order to obtain terminal conditions: $\boldsymbol{u}'_0\mapsto\boldsymbol{u}'_\tau$ by integration of (11) and $\boldsymbol{u}^*_\tau\mapsto\boldsymbol{u}^*_0$ by integration of (12). The terminal conditions at time τ are linked via (13).

The variation of the Lagrangian functional with respect to the initial condition $\boldsymbol{u}'_0$ can be written as

$$\frac{\delta L_0}{\delta\boldsymbol{u}'_0}=\left(\boldsymbol{u}^*_0-\frac{2(\boldsymbol{u}'_\tau,\boldsymbol{u}'_\tau)}{(\boldsymbol{u}'_0,\boldsymbol{u}'_0)^2}\boldsymbol{u}'_0,\delta\boldsymbol{u}'_0\right). \tag{14}$$

Using the definition of the gradient of the Lagrangian associated with the Gâteaux differential, the gradient of the Lagrangian functional with respect to the initial condition $\boldsymbol{u}'_0$ is

$$\nabla_{\boldsymbol{u}'_0}\mathcal{L}_0=\boldsymbol{u}^*_0-\frac{2(\boldsymbol{u}'_\tau,\boldsymbol{u}'_\tau)}{(\boldsymbol{u}'_0,\boldsymbol{u}'_0)^2}\boldsymbol{u}'_0. \tag{15}$$

A gradient minimisation method is used to optimise $\boldsymbol{u}'_0$ in order to reach maxima of G, i.e. where the gradient in (15) is zero and simultaneously where conditions (11–13) are satisfied. The algorithm is indicated schematically in figure 3; a similar representation can be found in [15]. Starting from an initial guess for the spatial distribution of $\boldsymbol{u}'_0$, the loop is iterated until the gradient (15) reaches an acceptably small level, in which case the gain G is estimated from the definition (3) using the final distributions for $\boldsymbol{u}'_0$ and $\boldsymbol{u}'_\tau$. An optimal step length for the gradient minimisation is obtained by exploiting linearity feature of the governing equations to update $\boldsymbol{u}'_0$ during the optimisation process [7, 14].

Eigenvalue approach

The eigenvalue approach to finding optimal initial perturbations for arbitrary flows was outlined in [1] and applied in [2, 4, 5, 12].

We may formalise the time integrations $\boldsymbol{u}'_0\mapsto\boldsymbol{u}'_\tau$ $\boldsymbol{u}^*_\tau\mapsto\boldsymbol{u}^*_0$ as operators so that

$$\boldsymbol{u}'_\tau=\mathcal{M}_0\boldsymbol{u}'_0 \qquad\text{and}\qquad \boldsymbol{u}^*_0=\mathcal{M}_0^*\boldsymbol{u}^*_\tau, \tag{16}$$

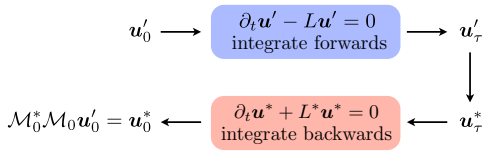

Figure 4: Application of the joint operator $\mathcal{M}_0^*\mathcal{M}$ to an initial vector $\boldsymbol{u}'_0$ used in the eigenvalue approach to calculating optimal initial perturbations. See also [1].

where the actions of $\mathcal{M}_0$ and $\mathcal{M}_0^*$ are obtained by temporal integration, respectively forwards and backwards over the interval $[0,\tau]$. Comparing the two forms of the Lagrangian functional (9) and (10), using (16), and the fact that $\boldsymbol{u}'$ and $\boldsymbol{u}^*$ must satisfy (11) and (12), we see that

$$(\boldsymbol{u}^*_\tau, \mathcal{M}_0\boldsymbol{u}'_0) = (\mathcal{M}_0^*\boldsymbol{u}^*_\tau, \boldsymbol{u}'_0).$$

Therefore $\mathcal{M}_0^*$ is the adjoint operator of $\mathcal{M}_0$ with respect to the inner product $(\cdot,\cdot)$. Substituting $\mathcal{M}_0$ into the Lagrangian functional and using this property, we now see that the Lagrangian can be expressed as a function only of $\boldsymbol{u}'_0$:

$$\mathcal{L}_0 = \frac{(\boldsymbol{u}'_\tau, \boldsymbol{u}'_\tau)}{(\boldsymbol{u}'_0, \boldsymbol{u}'_0)} = \frac{(\mathcal{M}_0\boldsymbol{u}'_0, \mathcal{M}_0\boldsymbol{u}'_0)}{(\boldsymbol{u}'_0, \boldsymbol{u}'_0)} = \frac{(\boldsymbol{u}'_0, \mathcal{M}_0^*\mathcal{M}_0\boldsymbol{u}'_0)}{(\boldsymbol{u}'_0, \boldsymbol{u}'_0)}. \quad (17)$$

Clearly the maximum value of the Lagrangian functional is the largest eigenvalue of the symmetric operator $\mathcal{M}_0^*\mathcal{M}_0$, and the corresponding eigenvector is the optimal initial perturbation.

The eigenvalues/eigenvectors of the operator $\mathcal{M}_0^*\mathcal{M}_0$ can be calculated by building a Krylov sequence through iteratively integrating a random initial perturbation forwards via the LNS equations, backwards via the ANS equations, and then using an Arnoldi method to extract the leading eigenvalues/eigenvectors [1]. Application of the joint operator $\mathcal{M}_0^*\mathcal{M}_0$ to an initial vector as one of a sequence of such applications is illustrated in figure 4.

If the matrix form of the forward operator $\mathcal{M}_0$ were available, one could alternatively obtain the optimal initial perturbation, optimal energy growth and optimal response from the singular value decomposition of $\mathcal{M}_0$:

$$\mathcal{M}_0\boldsymbol{U}_{0i} = \sigma_{0i}\boldsymbol{V}_{0i}. \quad (18)$$

The right and left singular vectors $\boldsymbol{U}_{0i}$ and $\boldsymbol{V}_{0i}$ form two orthogonal bases, normalised so that $(\boldsymbol{U}_{0i}, \boldsymbol{U}_{0i}) = 1$ and $(\boldsymbol{V}_{0i}, \boldsymbol{V}_{0i}) = 1$. The singular values σ_i are real and positive. The largest singular value is the square root of the optimal energy growth G and the corresponding right and left singular vectors are the optimal initial perturbation and the optimal outcome. This singular value decomposition approach is a direct method and only the forward operator $\mathcal{M}_0$ is involved. In general, the matrix corresponding to the action of $\mathcal{M}_0$ after spatial and temporal discretization is not available and so, as outlined above, iterative methods that rely only on applying operators have to be adopted.

By considering second variations, one may further show formally that converged optimal initial perturbations computed using the eigenvalue and optimisation approaches are equivalent.

Optimal boundary perturbations

In this section, we present a methodology to compute the other type of optimal perturbations considered in this work — optimal Dirichlet-type boundary perturbations that maximise the energy of the response perturbation field over a fixed time interval. In the following, we denote the segment of the boundary where the perturbation is introduced as the perturbation boundary. When calculating optimal boundary perturbations, the initial condition of the perturbation is set to be zero within the domain, i.e. $\boldsymbol{u}'_0 = 0$. Owing to the temporal form adopted for the perturbation boundary condition (4), the initial and boundary conditions do not conflict.

Optimisation approach

Analogously to the analysis of the optimal initial condition problem, a Lagrangian functional for the optimal boundary perturbation can be expressed as

$$\mathcal{L}_c = \frac{(\boldsymbol{u}'_\tau, \boldsymbol{u}'_\tau)}{[\hat{\boldsymbol{u}}_c, \hat{\boldsymbol{u}}_c]} - \langle \boldsymbol{u}^*, \partial_t\boldsymbol{u}' - L(\boldsymbol{u}')\rangle, \quad (19)$$

where the first term is the gain to be maximised and the second term applies the constraint of the LNS equation.

Setting the adjoint velocity variables to zero on the boundary, $\boldsymbol{u}^*(\partial\Omega) = 0$, and using zero initial conditions, we integrate the second term by parts to obtain

$$\mathcal{L}_c = \frac{(\boldsymbol{u}'_\tau, \boldsymbol{u}'_\tau)}{[\hat{\boldsymbol{u}}_c, \hat{\boldsymbol{u}}_c]} + \langle \boldsymbol{u}', \partial_t\boldsymbol{u}^* + L^*(\boldsymbol{u}^*)\rangle - (\boldsymbol{u}^*_\tau, \boldsymbol{u}'_\tau) + \left[\int_0^\tau f(t,\omega)(p^*\boldsymbol{n} - Re^{-1}\boldsymbol{\nabla_n}\boldsymbol{u}^*)\,\mathrm{d}t, \hat{\boldsymbol{u}}_c\right]. \quad (20)$$

In previous studies of local optimal boundary perturbations [6, 7, 9], the integration in the last expression of (20) vanishes because the pressure and a velocity component are eliminated through algebraic manipulations of the localised governing equations and both zero-Dirichlet and zero-Neumann conditions were enforced on the adjoint velocity components on the perturbation boundary. In studies when the pressure term cannot be eliminated analytically, this integral has to be taken into account. In the methodology to calculate the global optimal inflow perturbation for a stenotic flow presented in [11], a zero pressure condition was imposed on the inflow boundary to simplify the calculation. In the current work, a computed Neumann pressure boundary condition is adopted so as to relax the zero pressure simplification; such boundary conditions are consistent with a velocity correction scheme [3].

Setting to zero the first variations of $\mathcal{L}_c$ with respect to its independent variables $\boldsymbol{u}'$, $\boldsymbol{u}^*$ and $\boldsymbol{u}'_\tau$ yields the following set of equations:

$$\frac{\delta\mathcal{L}_c}{\delta\boldsymbol{u}^*} = 0 \quad \Longrightarrow \quad \partial_t\boldsymbol{u}' - L(\boldsymbol{u}') = 0, \quad (21)$$

$$\frac{\delta\mathcal{L}_c}{\delta\boldsymbol{u}'} = 0 \quad \Longrightarrow \quad \partial_t\boldsymbol{u}^* + L^*(\boldsymbol{u}^*) = 0, \quad (22)$$

$$\frac{\delta\mathcal{L}_c}{\delta\boldsymbol{u}'_\tau} = 0 \quad \Longrightarrow \quad \boldsymbol{u}^*_\tau = \frac{2\boldsymbol{u}'_\tau}{[\hat{\boldsymbol{u}}_c, \hat{\boldsymbol{u}}_c]}. \quad (23)$$

In the above, (21) are the LNS equations as previously defined in equation (1), which evolve the velocity perturbation $\boldsymbol{u}_c$ forwards in time from $t = 0$ to $t = \tau$ but now subject to inhomogeneous boundary conditions, (22) are the adjoint equations, which evolve the adjoint velocity $\boldsymbol{u}^*_\tau$ backwards from $t = \tau$ to $t = 0$, while (23) scales the outcome of the LNS equations at time $t = \tau$ in order to initialise the adjoint equations. The gradient of the Lagrangian functional with respect to the spatial distribution of the boundary condition $\hat{\boldsymbol{u}}_c$ can be expressed as

$$\nabla_{\hat{\boldsymbol{u}}_c}\mathcal{L}_c = \frac{-2(\boldsymbol{u}'_\tau, \boldsymbol{u}'_\tau)}{[\hat{\boldsymbol{u}}_c, \hat{\boldsymbol{u}}_c]^2}\hat{\boldsymbol{u}}_c + \boldsymbol{g}(\boldsymbol{u}^*, p^*, \omega), \quad (24)$$

where

$$\boldsymbol{g}(\boldsymbol{u}^*, p^*, \omega) = \int_0^\tau f(t,\omega)(p^*\boldsymbol{n} - Re^{-1}\boldsymbol{\nabla_n}\boldsymbol{u}^*)\,\mathrm{d}t. \qquad (25)$$

Thus the methodology required to compute the optimal spatial boundary perturbation distribution is conceptually rather similar to that employed for the computation of optimal initial conditions (see figure 3) except that the optimisation update now employs (24) instead of (15) and involves accumulating the integral (25), a vector function of spatial location along the perturbation boundary, during backward integration of (22).

We note that for the perturbation boundary, other valid combinations of boundary conditions exist for the adjoint velocity variables besides the zero Dirichlet condition, e.g.

$$\nabla_{\boldsymbol{n}}\boldsymbol{u}^* + \frac{Re\,p' - \nabla_{\boldsymbol{n}}\boldsymbol{u}'}{\boldsymbol{u}'}\boldsymbol{u}^* = 0, \quad \text{with} \quad p^* = 0, \qquad (26)$$

where the factor $(Re\,p' - \nabla_{\boldsymbol{n}}\boldsymbol{u}')/\boldsymbol{u}'$ — calculated component-by-component so that each term in this ratio is scalar — is calculated and stored in the forward integration of (21) and substituted into the Robin condition (26) at every time step during the backward integration of (22).

For this boundary condition the definition of $\boldsymbol{g}$ becomes

$$\boldsymbol{g}(\boldsymbol{u}^*, p', \omega) = \int_0^\tau f(t,\omega)(-\boldsymbol{n}\cdot\boldsymbol{U})\boldsymbol{u}^*\,\mathrm{d}t.$$

This 'outflow' type condition on the adjoint variable might be considered as more appropriate if the perturbation boundary is the inflow boundary and one follows the heuristic argument that the 'inflow' boundary for the LNS equations is an 'outflow' boundary condition for the adjoint equations owing to the change in sign of the advection terms. It has been demonstrated however that both sets of boundary conditions lead to the same value of gain [11]. This combination of boundary conditions also requires extra memory (to store $(Re\,p' - \nabla_{\boldsymbol{n}}\boldsymbol{u}')/\boldsymbol{u}'$) and more computer time owing to the update of the Robin condition for velocities in the backward integration. Therefore in the present work we did not employ this combination but instead took $\boldsymbol{u}^* = 0$ as noted above.

To summarise the initial and boundary conditions used in the optimal boundary condition problem, we adopt the following approach. The initial condition for the LNS equations is $\boldsymbol{u'}_0 = 0$ on the interior of the domain Ω. For evolution of the adjoint equations, the initial adjoint state (at time τ), $\boldsymbol{u'}_\tau$, is computed from (23).

On the perturbation boundary segment of $\partial\Omega$, we have Dirichlet boundary conditions on the perturbation velocity: $\boldsymbol{u'} = \boldsymbol{u'}_c = \hat{\boldsymbol{u}}_c f(t,\omega)$ in which the temporal function $f(t,\omega)$ is prescribed, and the spatial function $\hat{\boldsymbol{u}}_c$ is the object to optimise. On this segment the adjoint boundary conditions are prescribed to be $\boldsymbol{u}^* = 0$, while for pressure variables we adopt consistent Neumann pressure conditions [10], which do not impose any additional restraints on the equations.

The specification of initial and boundary conditions for the LNS and adjoint equations imposes some constraints on the temporal function $f(t,\omega)$. We see that the initial condition for the LNS equations is set to zero, so the Dirichlet velocity condition on the perturbation boundary at $t = 0$ has to be zero to eliminate the spatial discontinuity at the beginning of the forward integration. Further, since we require zero Dirichlet velocity conditions on the perturbed boundary for the adjoint equations, the initial condition for the adjoint equations, which is scaled from the final condition of the LNS equations by (23), has to be zero on the perturbation boundary, and therefore the final condition $\boldsymbol{u'}(\tau)$ has to be zero on the perturbation boundary, which requires $\boldsymbol{u'}_c = 0$ at $t = \tau$. To satisfy these compatibility requirements, the time-dependency function should satisfy $f(0,\omega) = f(\tau,\omega) = 0$.

The outflow boundary segment deserves additional attention. We can use $\boldsymbol{u'} = 0$ for $m \neq 0$, as presented in [11], but at $m = 0$, the mass flux into the domain from the perturbation boundary may be non-zero, and so a zero-Dirichlet outflow condition violates the mass conservation law. A new outflow boundary condition may be adopted to avoid this violation. For the forward integration it is a typical zero-Neumann outflow condition: $\nabla_n\boldsymbol{u'} = 0$, $p' = 0$, while for the backward integration it is a Robin condition, $\nabla_n\boldsymbol{u}^* + Re\boldsymbol{U}_n\boldsymbol{u}^* = 0$, $p' = 0$. Inspecting equation (8), one notes that the integral over the outflow boundary under these specifications is zero. At $m \neq 0$, the zero-Dirichlet outflow boundary condition and the new condition yield the same result within machine precision, providing that the computational domain is adequately long for the perturbation not to leave the domain. However, this new outflow condition (Neumann for forward integration and Robin for backward integration) is suitable for general-sized domains.

For the remaining boundaries, the boundary condition for the LNS equations and adjoint equations are the same. For example, on a cylindrical axis boundaries, the boundary conditions for velocity and pressure variables are zero-Dirichlet or zero-Neumann, depending on the azimuthal wave numbers, as outlined in [3] in combinations that also make no contribution to the integral term in equation (8); on far-field segments, zero Dirichlet velocity conditions and computed Neumann pressure conditions are adopted for the velocity components and pressure term in both LNS equations and the adjoint equations.

Eigenvalue approach

The boundary perturbation optimisation problem can be also transformed into an eigenvalue problem. Similar to the analysis of the optimal initial condition problem, we denote $\mathcal{M}_c$ as an evolution operator such that

$$\boldsymbol{u'}_\tau = \mathcal{M}_c\hat{\boldsymbol{u}}_c, \qquad (27)$$

with dual operator $\mathcal{M}_c^*$

$$\boldsymbol{g} = \mathcal{M}_c^*\boldsymbol{u}_\tau^*. \qquad (28)$$

Comparing the Lagrangian functional before and after the integration by parts as shown in (19) and (20), we note that $\mathcal{M}_c$ and $\mathcal{M}_c^*$ satisfy a duality relation arising from the last two terms in equation (20)

$$(\boldsymbol{a}, \mathcal{M}_c\boldsymbol{b}) = [\mathcal{M}_c^*\boldsymbol{a}, \boldsymbol{b}] \quad \text{where} \quad \boldsymbol{a} \in \Omega, \boldsymbol{b} \in \partial\Omega. \qquad (29)$$

Using relationships (27–29) in the Lagrangian functional, we obtain

$$\mathcal{L}_c = \frac{(\boldsymbol{u'}_\tau, \boldsymbol{u'}_\tau)}{[\hat{\boldsymbol{u}}_c, \hat{\boldsymbol{u}}_c]} = \frac{[\mathcal{M}_c^*\mathcal{M}_c\hat{\boldsymbol{u}}_c, \hat{\boldsymbol{u}}_c]}{[\hat{\boldsymbol{u}}_c, \hat{\boldsymbol{u}}_c]}.$$

Clearly the maximum value of $\mathcal{L}_c$ and the corresponding optimal boundary perturbation are the largest eigenvalue of the operator $\mathcal{M}_c^*\mathcal{M}_c$ and the associated eigenvector.

Recalling (23) and using (27) and (28), we observe that the joint action of $\mathcal{M}_c$ and $\mathcal{M}_c^*$ on the boundary perturbation $\hat{\boldsymbol{u}}_c$ can be expressed as

$$\mathcal{M}_c^*\mathcal{M}_c\hat{\boldsymbol{u}}_c = \mathcal{M}_c^*\boldsymbol{u'}_\tau = \boldsymbol{g}\frac{[\hat{\boldsymbol{u}}_c, \hat{\boldsymbol{u}}_c]}{2}. \qquad (30)$$

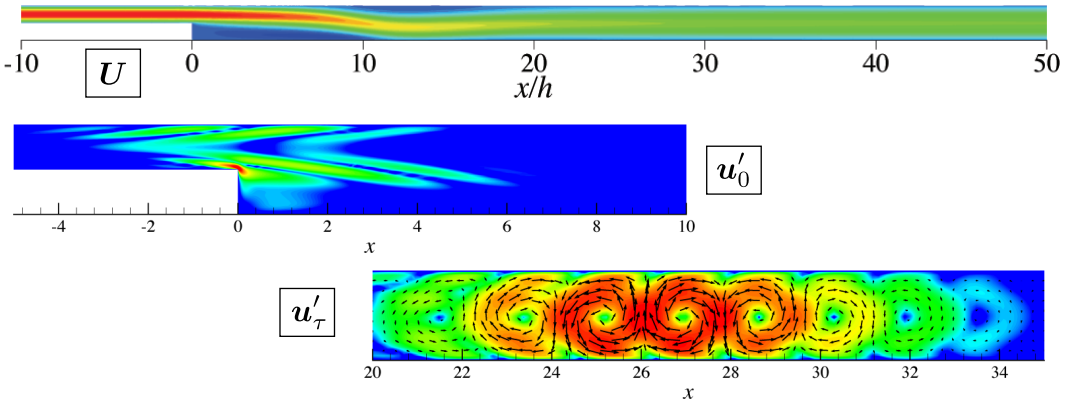

Figure 5: Example computation of an optimal initial condition for steady flow over a backward-facing step [2]. Steady base flow $\boldsymbol{U}$ at $Re = 500$, kinetic energy distribution of the two-dimensional global optimal initial condition $\boldsymbol{u'}_0$ for $\tau = 58$, and the corresponding outcome $\boldsymbol{u'}_\tau$.

Therefore when $\hat{\boldsymbol{u}}_c$ becomes the leading eigenvector of $\mathcal{M}_c^*\mathcal{M}_c$, $\boldsymbol{g}$ is parallel to the vector $\hat{\boldsymbol{u}}_c$ and the corresponding eigenvalue is $[\boldsymbol{g},\hat{\boldsymbol{u}}_c]/2$.

It can be demonstrated that the Lagrangian functional $\mathcal{L}_c$ has only one maximiser, which is the leading eigenvector of $\mathcal{M}_c^*\mathcal{M}_c$, where the maximum value of $\mathcal{L}_c$ is the corresponding largest eigenvalue; and only one minimiser, provided by the eigenvector associated with the smallest eigenvalue of $\mathcal{M}_c^*\mathcal{M}_c$, which is the minimum value of $\mathcal{L}_c$. All other eigenvectors of $\mathcal{M}_c^*\mathcal{M}_c$ correspond to inflection points of the Lagrangian functional.

Therefore an eigenvalue solver can be employed as an alternative to the optimisation method to calculate the optimal boundary perturbation. We start from an initial guess of the boundary perturbation, evolve it forwards in the LNS equations, use the final condition to initialise the adjoint LNS equation, evolve the adjoint variable backwards to obtain $\boldsymbol{g}$ (which must be evaluated throughout the integration interval), and then use $\boldsymbol{g}$ to initialise the LNS equations to repeat this cycle. This iterative action of the joint operator on the initial boundary perturbation builds a Krylov sequence and an Arnoldi method can be used to extract the eigenvalue/vectors of the joint operator from the sequence. The inner loop of the eigenvalue solver for the optimal boundary perturbation is conceptually similar to the inner loop for the optimal initial condition eigenvalue counterpart, illustrated in figure 4.

Analogously to the case for the optimal initial perturbation discussed earlier, if the matrix form of the forward operator $\mathcal{M}_c$ is available, we can obtain the optimal boundary perturbation, optimal gain and optimal response from the singular value decomposition of $\mathcal{M}_c$:

$$\mathcal{M}_c\boldsymbol{U}_{ci} = \sigma_{ci}\boldsymbol{V}_{ci}. \tag{31}$$

The right and left singular vectors $\boldsymbol{U}_{ci}$ and $\boldsymbol{V}_{ci}$ form two orthogonal bases, and they are normalised so that $[\boldsymbol{U}_{ci},\boldsymbol{U}_{ci}] = 1$ and $(\boldsymbol{V}_{ci},\boldsymbol{V}_{ci}) = 1$. The singular values σ_{ci} are real and positive. Clearly the largest singular value is the square root of the optimal gain and the corresponding right and left singular vectors are the optimal boundary perturbation and the optimal outcome. This singular value decomposition approach is a direct method and only the forward operator $\mathcal{M}_c$ is involved. In general global studies, the matrix form of $\mathcal{M}_c$ is not available and an iterative method such as an optimisation or eigenvalue method must be adopted to calculate the optimal boundary perturbation.

Case studies

Our case study results are all computed using spectral element spatial discretisations with a backward-difference time integration scheme see e.g. [3]. However the general characteristics of the results obtained would be much the same regardless of the discretisations employed.

Optimal initial perturbation

An example that illustrates the global optimal initial condition computed for two-dimensional perturbations to two-dimensional flow over a backward-facing step is shown in figure 5, where the energy growth $G = 63.1 \times 10^3$ for $\tau = 58.0$ [2]. While for any time horizon τ the methods deliver the optimal initial perturbation $\boldsymbol{u'}$ and growth G, in flows where the perturbation is asymptotically stable for large times, one has to find the value of τ which delivers largest overall growth (the global optimum) by trial and error, since linear perturbation energies will eventually fall to zero in the $\tau \to \infty$ limit.

The iteration convergence of optimal energy growth G for both methods (though for a different problem) are compared in figure 6. The convergence criterion for the optimal energy growth is defined as $r_{0\text{value}} = (G^k - G^{40})/G^{40}$ where the superscript denotes iteration index. We see that the eigenvalue method converges much more rapidly than the optimisation method. The amount of work per iteration is similar for the two methods, so the eigenvalue approach is clearly superior for this optimal initial perturbation problem.

Optimal boundary perturbation

An example which illustrates the outcomes of an optimal boundary perturbation computation was presented in [11], which deals with inflow boundary perturbations to steady stenotic flow. The optimal initial conditions and outcomes for this flow were earlier presented in [4] and form an interesting basis for comparison. The nature of the temporal dependence of the inflow perturbations employed, a type of burst signal, is illustrated in figure 2; the frequency of the oscillation was initially selected using knowledge of the optimal initial condition outcome.

Figure 7 shows outcomes of an optimal boundary condition computation for steady stenotic flow at $Re = 400$, azimuthal wavenumber $m = 1$ (which provides the largest energy growth G and gain K), and time horizon $\tau = 6.71$.

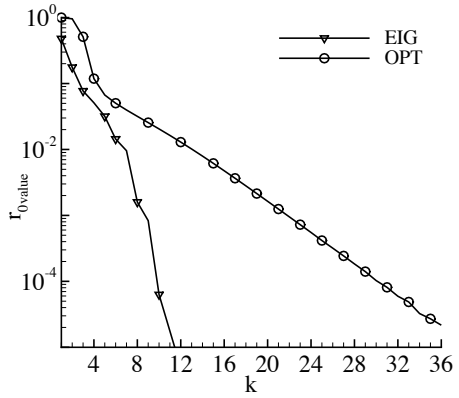

Figure 6: Comparison of convergence of optimal energy growth G for the optimisation method and eigenvalue method applied to an example initial condition problem; k is loop iteration index.

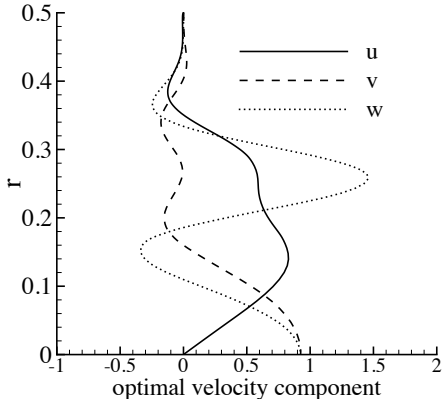

Figure 7: Radial profiles of optimal inflow boundary condition perturbation computed for steady stenotic flow at $Re = 400$, $m = 1$, $\tau = 6.71$. The velocity components (u, v, w) respectively represent axial, radial and azimuthal flow speeds. See also [11].

The perturbation flow that evolves downstream from this inflow boundary condition disturbance is illustrated in figure 8. As noted in [11], this perturbation flow is extremely similar to the result of an optimal initial disturbance at the time for global maximum energy growth. The perturbation evolves to a sinuous disturbance of the axisymmetric shear layer present in the base flow at this location, which in turn results from flow separation in the stenosis throat.

The temporal evolution resulting from the same boundary condition perturbation is illustrated in figure 9, where contour levels are chosen arbitrarily in order to show structure. We see that at $t = 1.98$, the inflow pulse, while still not fully advected into

Figure 8: Positive/negative isosurfaces of axial velocity perturbation to steady stenotic flow at time of maximum gain, $t = \tau = 6.71$ resulting from the inflow boundary perturbation shape shown in figure 7.

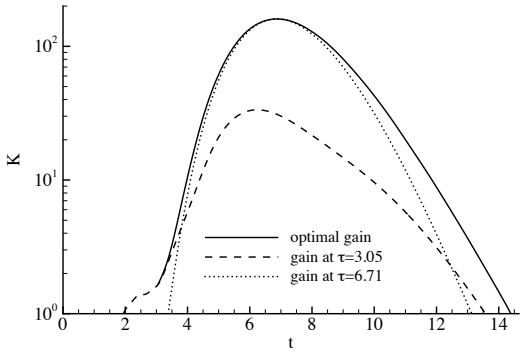

Figure 10: Optimal gain envelope for an inflow perturbation to steady stenotic flow for $Re = 400$, azimuthal wavenumber $m = 1$, together with the time evolution of transient gains with optimal inflow perturbations specific to $\tau = 3.05$ and $\tau = 6.71$.

the domain, has reached the stenosis throat, and there develops structure that is locally similar to the optimal initial condition on the shear layer adjacent to the contraction (compare to figure 5 *b* of [4]).

Analogously to optimal initial condition studies of linearly stable flows, for any given boundary perturbation time profile $f(t, \omega)$, there is an associated time horizon τ_{opt} that gives global optimal gain K. In order to find the global optimal gain and the associated time horizon, the method presently under discussion requires that τ_{opt} must be established by another level of optimisation, or on a trial-and-error basis. This point is illustrated in figure 10, which shows the envelope of optimal gain as a function of time horizon τ. Each computation for K at given τ finds one point on the envelope. Linear evolution of the gain with time for any particular optimal boundary perturbation associated with this τ falls within the envelope, osculating it at the corresponding τ. In this case, $\tau_{opt} = 6.71$with the associated global optimal gain $K = 159.4$.

Finally we consider the relative performance of the optimisation and eigenvalue approaches to computing optimal boundary disturbances. The convergence speeds of the optimal gain for both optimisation method and eigenvalue method are reported in figure 11. The convergence criterion for gain is defined as $r_{cvalue} = (K^k - K^{10})/K^{10}$, where the superscript denotes the index of iterations. We see that in contrast to what was observed for the calculation of optimal initial conditions, the optimisation method ultimately converges a faster than the eigenvalue method. This is because of the low dimension of the operator $\mathcal{M}_c^* \mathcal{M}_c$, related to the fact that here the optimisation task (over a boundary surface) is of lower dimensionality than for an optimal initial perturbation problem (over a spatial volume).

Conclusions

These discussion reveal some of the underlying similarities between the conceptual frameworks used for the study of optimal initial and boundary condition disturbances in arbitrary open flows, as well as physical outcomes. Either optimisation-based or eigensystem-based methods may be employed for computations, though as the dimensionality of the problem increases — from boundary surface to spatial volumetric disturbances — iterative (Arnoldi-type) eigensystem computations have been more efficient than (steepest-descent) optimisation methods.

The connection between the physics of optimal boundary and initial perturbations is strong, as was also suggested (via DNS)

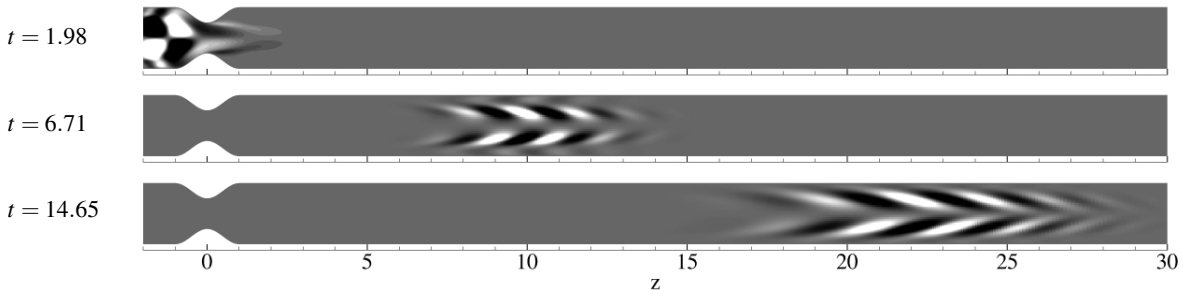

Figure 9: Time evolution resulting from the optimal inflow boundary perturbation to steady stenotic flow at $Re = 400$, $m = 1$, $\tau = 6.71$. Contours of axial velocity component on the meridional plane; contour levels are chosen arbitrarily to highlight the structure of perturbation flows and differ in each panel. The equivalent perspective view for $t = 6.71$ is shown in figure 8.

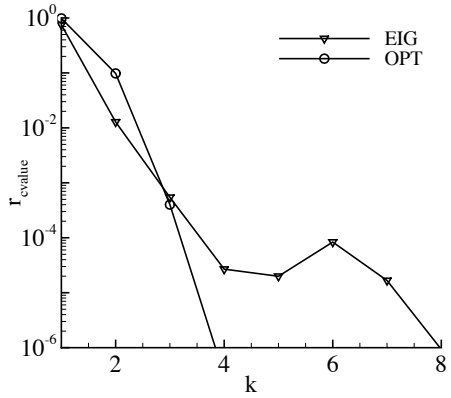

Figure 11: Comparison of convergence of optimal gain K for the optimisation method and eigenvalue method applied to the computation of boundary condition perturbations in an example flow; k is loop iteration index.

in previous studies [1, 2, 5]. Informally, we can conceptualise the process of optimal boundary perturbations in open flows as being closely related to that for optimal initial perturbations, whereby the boundary perturbation advects to the zone for the optimal initial perturbation, convolves with its distribution, with the subsequent physics being essentially those resulting from an optimal initial perturbation. Firmly establishing the formal connection remains an open problem.

Acknowledgements

We would like to acknowledge financial support from the Australian Research Council through Discovery Program Grant DP1094851, and from Australia's National Computational Infrastructure via Merit Allocation Scheme Grant D77. SJS would like to acknowledge financial support under EPSRC grant EP/H050507/1.

References

[1] Barkley, D., Blackburn, H. M. and Sherwin, S. J., Direct optimal growth analysis for timesteppers, *Intnl J. Num. Meth. Fluids*, **57**, 2008, 1437–1458.

[2] Blackburn, H. M., Barkley, D. and Sherwin, S. J., Convective instability and transient growth in flow over a backward-facing step, *J. Fluid Mech.*, **603**, 2008, 271–304.

[3] Blackburn, H. M. and Sherwin, S. J., Formulation of a Galerkin spectral element–Fourier method for three-dimensional incompressible flows in cylindrical geometries, *J. Comput. Phys.*, **197**, 2004, 759–778.

[4] Blackburn, H. M., Sherwin, S. J. and Barkley, D., Convective instability and transient growth in steady and pulsatile stenotic flows, *J. Fluid Mech.*, **607**, 2008, 267–277.

[5] Cantwell, C. D., Barkley, D. and Blackburn, H. M., Transient growth analysis of flow through a sudden expansion in a circular pipe, *Phys. Fluids*, **22**, 2010, 034101–1–15.

[6] Corbett, P. and Bottaro, A., Optimal control of nonmodal disturbance in boundary layers, *Theoret. Comput. Fluid Dynamics*, **15**, 2001, 65–81.

[7] Guégan, A., Schmid, P. J. and Huerre, P., Optimal energy growth and optimal control in swept Hiemenz flow, *J. Fluid Mech.*, **566**, 2006, 11–45.

[8] Gunzburger, M. D., *Perspectives in Flow Control and Optimization*, SIAM, 2000.

[9] Hogberg, M. and Henningson, D. S., Linear optimal control applied to instabilities in spatially developing boundary layers, *J. Fluid Mech.*, **470**, 2002, 151–179.

[10] Karniadakis, G. E., Israeli, M. and Orszag, S. A., High-order splitting methods for the incompressible Navier–Stokes equations, *J. Comput. Phys.*, **97**, 1991, 414–443.

[11] Mao, X., Blackburn, H. M. and Sherwin, S. J., Optimal inflow boundary condition perturbations in steady stenotic flows, *J. Fluid Mech.*, **705**, 2012, 306–321.

[12] Mao, X., Sherwin, S. J. and Blackburn, H. M., Transient growth and bypass transition in stenotic flow with a physiological waveform, *Theoret. Comput. Fluid Dynamics*, **25**, 2011, 31–42.

[13] Noack, B. W., Morzynski, M. and Tadmor, G., editors, *Reduced-Order Modelling for Flow Control*, Springer, 2011.

[14] Nocedal, J. and Wright, S., *Numerical Optimization*, Springer, 1999.

[15] Schmid, P. J., Nonmodal stability theory, *Annu. Rev. Fluid Mech.*, **39**, 2007, 129–162.